Journal of Bionic Engineering (2023) 20:1635–1645
https://doi.org/10.1007/s42235-023-00355-9

RESEARCH ARTICLE

Development of Bio-cultured Artificial Muscles with High Design Flexibility

Hirono Ohashi[1] · Shunsuke Shigaki[1] · Ryo Teramae[1] · Masahiro Shimizu[1] · Koh Hosoda[1]

Received: 15 September 2022 / Revised: 31 January 2023 / Accepted: 6 February 2023 / Published online: 13 March 2023

Abstract

Recent advances in bionics have made it possible to create various tissue and organs. Using this cell culture technology, engineers have developed a robot driven by three-dimensional cultured muscle cells (bioactuator)—a muscle cell robot. For more applications, researchers have been developed various tissues and organs with bio3D printer. However, three-dimensional cultured muscle cells printed by bio3D printer have been not used for muscle cell robot yet. The aim of our study is to develop easy fabrication method of bioactuator having high design flexibility like as bio3D printer. We fabricated three-dimensional cultured muscle cells using mold and dish having pin which can contribute to shape and cell alignment. In this study, we observed that our method maintained the shape of three-dimensional cultured muscle cells and caused cell alignment which is important for bioactuator development. We named three-dimensional cultured muscle cells developed in this study "bio-cultured artificial muscle (BiCAM)". Finally, we observed that BiCAM contracted in response to electrical stimulus. From these data, we concluded our proposed method is easy fabrication method of bioactuator having high design flexibility.

Keywords Three-dimensional cultured muscle cells · Bio-cultured artificial muscle · Skeletal muscle cell · Tissue engineering

1 Introduction

Artificial muscles inspired by living organisms and biological muscles have been developed for soft robotics [1, 2]. On the other hand, bio-hybrid robots incorporating biological materials have also been developed. Muscle cell robots are bio-hybrid robots that use muscle cells themselves as actuators. There are two types of muscle cell robots, one that uses cardiomyocytes and another that uses skeletal muscle cells [3–5]. Cardiomyocyte robots consist of cardiomyocytes arranged in a planar fashion on a base elastomer. Since the cardiomyocyte is an involuntary muscle, a muscle cell robot driven by this muscle is constantly moving [6–8]. In contrast, skeletal muscles are voluntary muscles. Therefore, a muscle cell robot driven by skeletal muscles can be powered on/off by external inputs such as electrical stimulation [9–14].

Skeletal muscle cell robots use three-dimensional cultured skeletal muscle cells as actuators, because cultured skeletal muscle is greater than that of their two-dimensional counterparts [15]. The former consists of myoblast and extracellular matrix (ECM), with muscle cells in a layered structure. The latter is a single layer of skeletal muscle cells, consisting only of myoblast. Myoblast is progenitor cell of muscle cell. Therefore, we need build muscle cells in three dimensions when skeletal muscle cells are used for robot actuator.

Muscle cell robots driven by a three-dimensional cultured skeletal muscle cells have been developed, but these actuator shapes remain rectangle and ring [10–14]. For more robotic application, more flexible design of a bioactuator is required. Researchers developed skeletal muscle tissue and/or other tissue with bio3D printer (bioprinting

✉ Hirono Ohashi
ohashi@arl.sys.es.osaka-u.ac.jp

Shunsuke Shigaki
shigaki@arl.sys.es.osaka-u.ac.jp

Ryo Teramae
teramae.ryo@arl.sys.es.osaka-u.ac.jp

Masahiro Shimizu
shimizu@sys.es.osaka-u.ac.jp

Koh Hosoda
hosoda@sys.es.osaka-u.ac.jp

[1] Department of Systems Innovation, Osaka University, 1-2, Machikaneyama, Toyonaka, Osaka 560-0043, Japan

technique) [16–18]. However, three-dimensional cultured muscle cells with bioprinting technique have been not used for muscle cell robot yet, because maintaining a bio3D printer for bioprinting requires tips from experience and huge cost. In addition, many researchers focus on clinical and edible use [16, 17, 19]. If any shape of bioactuator can be produced with same manufacturing process, it is expected to be standardized. From these things, we thought it is necessary to develop easy fabrication method of three-dimensional cultured skeletal muscle cells with high design flexibility like as bioprinting technique without bio3D printer.

Three-dimensional cultured muscle cells were also called bioactuators when it used in muscle cell robot [10, 12]. Muscle contraction in response to is an essential factor because bioactuators function by shrinking as same as biological muscle. Cell alignment is a key component for culture of three-dimensional cultured muscle cells because living skeletal muscle tissue has a highly organized structure consisting of long parallel myotubes which formed by differentiation and fusion of myoblasts [20]. In addition, as generation of a uniaxial force is the main purpose of skeletal muscle tissue [21], cell alignment is thought to be related to contraction force. Thus, cell alignment is also important for development of bioactuator.

Cellular responses to external stimuli have been used to induce cell alignment for improvement of bioactuators [21–26]. Heher et al. [21] cultured bioactuators while periodically applying a mechanical stretching stimulus. Muscle cells cultured with mechanical stimulation were aligned and expression levels of myogenesis marker were higher than other condition suggesting better maturation [21]. However, dynamic external stimuli require the use of various devices which increases the complexity of experimental process. Spontaneous contraction of the bioactuator during culture is utilized to simplify the application of mechanical stimulation. Huang et al. fabricated an actuator by dropping fibrin gel containing myoblast onto the entire surface of a dish with two pins erected in a straight line [22]. Due to spontaneous contraction during culture, the actuator deformed to connect the pins and cell alignment were induced. As a result, the cell alignment was observed. These indicate that mechanical stimulation, whether static or dynamic, contributes to the cell alignment of bioactuators. However, the shapes after maturation were not controlled by Huang et al. because tissue shape and cell alignment were determined by cell dynamics in response to two pins location. It means that the property of bio-actuator that can be made each time may vary. From these point, engineers need to be able to control the shape and the cell orientation in order to standardize bioactuators. In addition, the orientation of the cells and the shape of the bioactuator cannot be predicted when culturing tissue under more needles.

In order to develop a method to fabricate bioactuators with a high design flexibility, we propose an easy method to determine the shape of bioactuator while controlling the alignment of the muscle cells using mechanical stimuli. Specifically, we investigated whether we can control final tissue shape and cell orientation by adding a mold that determines the initial shape of the tissue to the method of Huang et al. In this study, we established three evaluation criteria that must be met in order to achieve the method. The criteria are follows—(i) can set/maintain a three-dimensional cultured skeletal muscle shape, (ii) can control a direction of cell alignment of a three-dimensional cultured skeletal muscle, (iii) the three-dimensional cultured skeletal muscle cells can function as actuator (contraction in response to external stimulus). We performed three experiments mainly to verify whether those criteria were met.

2 Design of Bioactuator Fabrication Method

2.1 Fabrication Flow of BiCAM

The three-dimensional cultured muscle cells produced in this study are called BiCAM (bio-cultured artificial muscle). A dish with pins and a plastic mold were used for our proposed method (Fig. 1a, b). The dish is consisted of a plastic base for setting pins and a silicon elastomer to fix base on a dish (Fig. 1a). The mold is a circle shape plastic board and has hole to form BiCAM shape (Fig. 1b). The BiCAM fabrication procedure is shown in Fig. 1c. The mold is placed in alignment with pins. Extracellular matrix (ECM) solution containing myoblasts is poured into the mold hole.

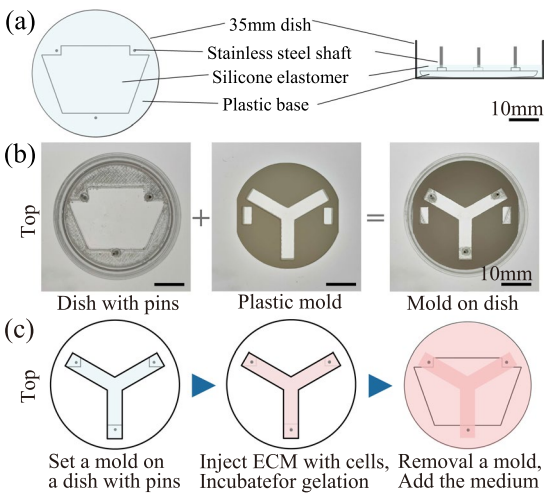

Fig. 1 Structure and fabrication procedure of the proposed method. **a** An overall view of a dish with pins. **b** An enlarged view of the dish, the plastic mold, and the mold and dish together. **c** Fabrication procedure of Y-shaped BiCAM

After gelation at 37°C, the mold is removed and a medium is added. When the hole shape is Y-shape, the BiCAM became Y-shaped (Fig. 1b right and 1c). The Y-shaped BiCAMs are cultured while fixing the three end points.

2.2 Action Mechanism of Proposed Method

Three-dimensional cultured muscle cells, which consist of myoblasts and ECM, have the property of spontaneously shrinking during the culture process, which is available for induction of cell alignment [22]. If three-dimensional cultured muscle cells are fixed during culture, spontaneously shrinking force is applied to the cells inside. This force becomes a mechanical stimulus to cells in the three-dimensional cultured muscle cells. It can be expected to promote the cell alignment. The direction of cell alignment is as same as mechanical stimulus direction.

Table 1 shows the conditions for the proposed method and the comparison group. Figure 2 shows the expected results for each condition. Proposed method is the presence of cells, pins, and a mold condition (Proposed; Table 1). In proposed condition (Fig. 2 fourth row), the end of the Y-shaped BiCAM is fixed by pins, which exerts long-axis tension in the BiCAM. As a result, the shape of the BiCAM, including its size, is maintained (Shape/Size: ○/○) and the alignment of cells in the long-axis direction is observed (Cell alignment: ○). Since biological muscles have cells aliment of the long-axis direction, the resulting muscle tissue is expected to be functional showing contraction in response external stimuli (Function: ○). In this study, we set three conditions as comparison: without cells (Cell−), without pins (Pins−), and without a mold (Mold−) (Table 1). The expected results are shown in Fig. 2. In the Cell− condition (Fig. 2 second row), the Y shape is maintained because spontaneous contraction by the cells does not occur (Shape/Size: ○/○). However, it does not function as a bioactuator due to the absence of myocyte (Function: X). In the Pins− condition (Fig. 2 third row), Y-shaped BiCAM shrinks (Shape/Size: ○/X). In particular, the long-axis direction shrinks significantly, so the cell alignment becomes short axis or random (Cell alignment: X). The contraction rate of muscle tissue in Pins− in response to external stimuli is reduced because of the shrinkage of the tissue itself and the lack of cell orientation. As a result, the function of the actuator is reduced (Function: △). In the Mold− condition (Fig. 2 fifth row), the shape of the BiCAM is not defined. Therefore, shrinkage by the cells occurs in random directions and the cell alignment is unpredictable. In other words, we cannot control the final shape or cell alignment and the tissue weakly contracts in response to external a stimuli (Shape: X, Cell alignment: X, Function: △). Based on the above, it is expected that BiCAM cultured by the proposed method will satisfy the three criteria set in this study: (i) shape maintenance, (ii) cell alignment, and (iii) contraction in response to external stimuli.

Table 1 Conditions of the proposed method and comparison groups

	Conditions	Cell	Pins	Mold
1	Cell−	−	−	+
2	Pins−	+	−	+
3	Proposed	+	+	+
4	Mold−	+	+	−

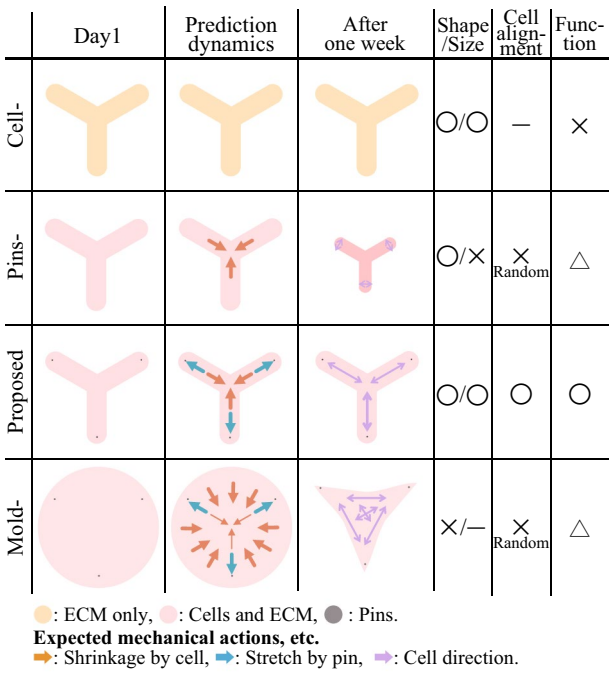

Fig. 2 Expected action mechanism and induced phenotype under each condition. Shape; ○: keep mold shape, X: can not keep. Size; ○: keep size, X: can not keep because of shrinkage, - not evaluated. Cell alignment; ○: long-axis cell alignment, X: dose not occur (random), - not evaluated. Function; ○: show contraction in response to external stimulus, X: show contraction some times or weak contraction in response to external stimulus, X: dose not work

3 Materials and Methods

3.1 Preparation of Dishes with Pins and Molds

The base for Y shape was made of acrylonitrile butadiene styrene (ABS) resin printed using a 3D printer. There are three needle holes. A needle spacing was 20.785 mm. The base was placed on a culture dish with a diameter of 35 mm, a pin (diameter: 0.8 mm, length: about 5 mm) was inserted into the needle hole of the base, and PDMS (polydimethylsiloxane, SILPOT 2184, DuPont Toray Specialty Materials K.K., Tokyo, Japan) was poured. This was then heated in

an oven to harden the PDMS. The base for I-shape has two needle holes and a needle spacing was 20 mm. The base was placed on a culture dish with a diameter of 100 mm, a pin (diameter: 0.8 mm, length: 8–10 mm) was inserted. After that, the same operation as the dish for Y-shape was performed. The stainless-steel wire or shaft was used as a pin.

The molds were made as follows: The Y-shaped mold was made by cutting a 3 mm thick polyoxymethylene plate with a laser cutter (mcn004, SmartDIYs, Yamanashi, Japan) into a circular plate with a Y-shape hole. The I-shaped mold was made in the same way as the Y-shaped mold. The hole of the I-shape mold was a rectangle of 3.5 mm × 25 mm.

3.2 Cell Lines

The myoblast line C2C12 (ATCC CRL-1772) purchased from American Type Culture Collection (ATCC, VA, USA) and C2C12 (RCB0987) purchased from RIKEN BRC (Ibaraki, Japan) were used.

3.3 Fabrication and Cultivation of BiCAM

The composition of the cell-containing ECM for analysis of shape maintenance (Y-shaped) was 3.0×10^6 myoblasts, 1000 µl Collagen (Cellmatrix I-A, Nitta Gelatin, Osaka, Japan). DMEM containing 10% fetal bovine serum (FBS, SH30088.03, HyClone, Cytiva, Tokyo, Japan), 1% penicillin–streptomycin (PS, 06168-34, Nacalai Tesque, Kyoto, Japan). 400 µl of ECM containing cells were used for one Y-shaped BiCAM. However, 600 µl of ECM containing cells were used to spread the material throughout the dish in the Mold− condition. 2–3 days after the BiCAM fabrication, the growth medium was switched to a differentiation medium (MYB-DM, Cosmo Bio Co., LTD., Tokyo, Japan). Differentiation medium was changed every 2–3 days. BiCAM was cultured in a CO_2 incubator at a temperature of 37 °C and a CO_2 concentration of 5%.

The composition of the cell-containing ECM for cell alignment and functional analysis was 3.0×10^6 myoblasts, 600 µl Matrigel (356237, Corning, NY, USA), 200 µl Fibrinogen (20 mg/ml, F3879, Sigma-Aldrich, USA), 40 µl Thrombin (50 Units in 1 ml, T7009, Sigma-Aldrich, MO, USA), and 164 µl growth medium. DMEM containing 10% FBS, 1% PS, and 1% 6-Aminocaproic acid (ACA, A2504, Sigma-Aldrich, MO, USA) was used as the growth medium. 200 µl of ECM containing cells were used for one I-shaped BiCAM. 2–3 days after the BiCAM fabrication, the growth medium was switched to a differentiation medium. Before use, insulin (I2643, Sigma-Aldrich, MO, USA) and ACA were added to differentiation medium. We referred to previous studies [13, 27] for the fundamental fabrication procedure, but we note that material ratio and cell density have been changed after trial and error.

3.4 Observation of Y-shaped BiCAM

Photographs of the overall view of BiCAM were taken on days 1, 3, and 10 to compare the shapes. In addition, a phase contrast microscope (IX73, Olympus, Tokyo, Japan) was used to observe cells in BiCAMs.

3.5 Analysis of I-shaped BiCAM Length

X-length is termed as length and Y-length is termed as width. The lengths and widths were measured using ImageJ [28] on days 1, 3, and 6. In addition, the rate of change on day 6 was calculated. The formula is as follows: Rate of change = ((Day6 − Day1)/Day1)*100.

3.6 Immunostaining for Myotube

BiCAM was cut into four–six pieces with a scalpel. The sections were washed with PBS (−) and allowed to stand at 4 °C for 1 h with 2% formaldehyde for fixation. The sections were washed with PBS and placed in PBST solution (PBS solution containing 0.5% Triton X-100 (160-24751, FUJIFILM Wako Pure Chemical Corp., Osaka, Japan)) at 23±5 °C for 5 min. After washing with PBS, the sections were immersed in 0.05% Triton X-100 citrate buffer (10 mM, pH 6.0) solution and boiled at 95 °C for 30 min to activate antigen [29]. The sections were subsequently immersed in a 0.3% PBST solution containing 4% BSA (015-27053, FUJIFILM Wako Pure Chemical Corp., Osaka, Japan) and left overnight at 4 °C. After washing, a solution of myosin heavy chain (MHC) primary antibody (MAB4470, R & D systems, Inc., MN, USA) diluted to 1/300 with PBST was added, and the mixture was allowed to stand at 37 °C for 1 h. After washing with PBS, donkey anti-Mouse IgG antibody (A32787, Invitrogen, MA, USA) solution diluted to 1/1000 with PBST was add. The sections were then allowed to stand in secondary antibody solution at 37 °C for 1 h. After washing, the sections were mounted with PBS, and fluorescence was observed using a confocal microscope (FV1200-IX83, Olympus, Tokyo, Japan). Two BiCAMs of Pins− condition and three BiCAMs of Pins+ condition were used for immunostaining.

3.7 Analysis of Cell Alignment

An analysis code (Python v3.8, Open CV) [30] was created for estimating cell alignment, using the images captured after immunostaining. The analysis was conducted with the direction of the pattern in the images as the alignment direction of the cells. We visualized cell alignment direction using a pseudo-color plot of Matlab because the image processing stores the cell alignment direction values as a matrix. Moreover, the data for alignment direction was visualized using a rose diagram in increments of 10°. The

Watson–Williams test was used to determine the difference in alignment distribution between the two conditions (Pins− and Pins+). The Watson–Williams test was run using the MATLAB Toolbox for Circular Statistics [31].

3.8 Electro-stimulation and Behavior Analysis

Electrical stimulation and behavioral analysis were conducted with reference to previous research [32, 33]. Platinum plates ($9 \times 30 \times 0.1$ mm) were inserted into both ends of the dish containing the medium and BiCAM. Colorless DMEM (040-30095, FUJIFILM Wako Pure Chemical Corp., Osaka, Japan) which does not contain phenol red, was used as the medium to make muscle observation easier. One pin was removed from the BiCAM. Electrical stimulation timing was controlled using a microcomputer (Arduino Uno, Arduino LLC, Italy) and a voltage application circuit (MD25HV, Cytron, Penang, Malaysia). The conditions of electrical stimulation given are 25 V/75 mm (electric field), 10 ms (duration time), and 1 or 50 Hz (input frequency). The stimuli were applied five times for 1 Hz and 250 times for 50 Hz. The BiCAM was recorded from above with a video camera. From the video, the change in BiCAM length was estimated by analyzing its endpoints using DeepLabCut [34]. Noise was removed from the raw data using a low-pass filter with a cut-off frequency of 5 Hz on MATLAB (R2020b, The MathWorks, Inc., MA, USA). The data without noise was used as the final data. The graphs were created with the start of stimulation as 0 s.

3.9 Statical Analysis

IBM SPSS Statistics (International Business Machines Corporation, NY, USA) was used for statistical analysis unless otherwise stated.

4 Results

4.1 The Proposed Method Can Form BiCAM Shape

To test our hypothesis, we first analyzed shape maintenance. We fabricated BiCAMs under four conditions (two samples/each condition). We observed BiCAM shape and cells inside tissue at days 1, 3, and 10. Figures 3 and 4 show results of BiCAM shape and cells inside tissue, respectively. The BiCAM cultured by the proposed method maintained its Y-shaped shape and size (Fig. 3 fourth row). The shape and size of BiCAM cultured under Cell− and Pins− conditions were also as expected as shown in Fig. 2. However, the Mold− condition did not show any tissue shrinkage, which was different from our expectation (Fig. 3 fifth row). Next, cells in the tissue were observed with a phase contrast

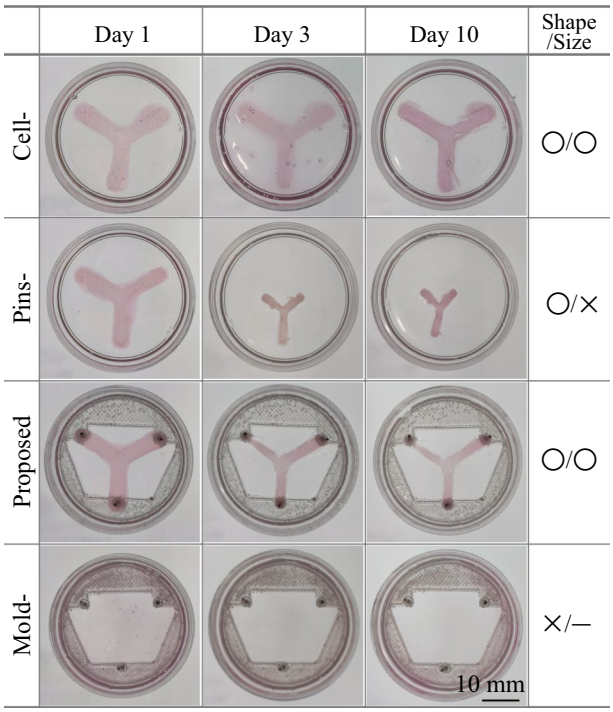

Fig. 3 Shape maintenance analysis using Y-shaped BiCAMs. Shape; ○: can keep mold shape, X: can not form. Size; ○: can keep size, X: can not keep because of shrinkage, -: can not be evaluated

microscope simply. Observations were made so that the longitudinal part of Y was aligned with the horizontal axis (Fig. 4a). In the Mold− condition, observations were made at the same location and in the same direction as in the other conditions, using the position of the needle as a guide. Any cells were not observed in BiCAM of the Cell− condition (Fig. 4b second row). Tissue shrinkage occurred in the Pins− condition, resulting in a bumpy surface that was only partially in focus and the cell alignment could not be determined (Fig. 4b third row). BiCAM of the proposed method showed cell alignment in the longitudinal axis as expected (Fig. 4b fourth row). In the Mold− condition, cells were clearly visible, unlike under the Proposed and Pins− conditions and the cell alignment was random(Fig. 4b fifth row). This may be due to the fact that the ECM containing cells was spread over the entire dish, resulting in less hierarchy than in the other conditions. This may also explain the lack of shrinkage by the cells. These results were common to all two samples in each condition.

For more detailed analysis, further experiments were performed using I-shaped BiCAMs. The experimental flow is shown in Fig. 5. The shape maintenance of BiCAM was investigated by measurement of the length of BiCAM (Fig. 6). The long-axis direction is defined as the x-axis, and the short-axis direction is defined as the y-axis (Fig. 6a, b). The length (x-length) and width (y-length) of four samples

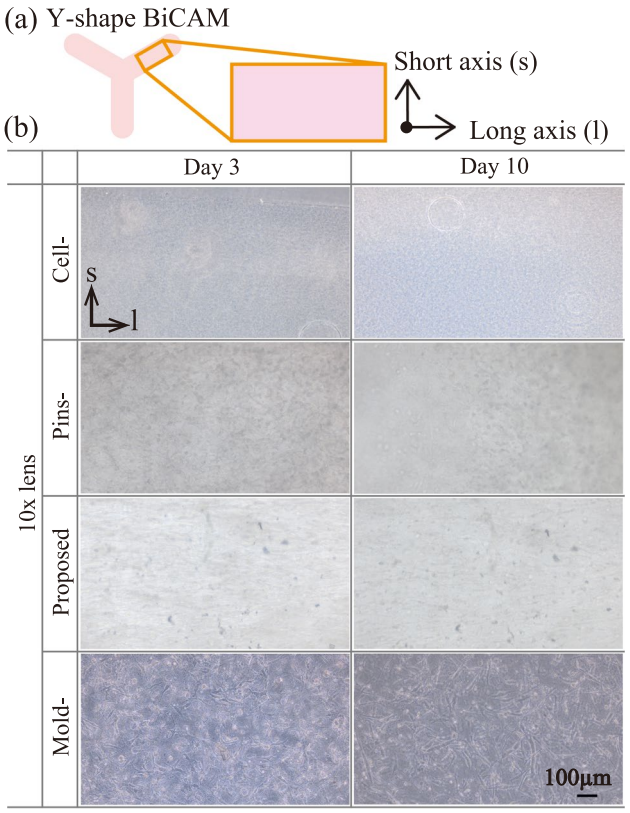

Fig. 4 Observation of muscle cells in BiCAM with phase contrast microscope. **a** Definition of observation axis observations were made so that the longitudinal part of Y was aligned with the horizontal axis. **b** Result on days 3 and 10 under each condition

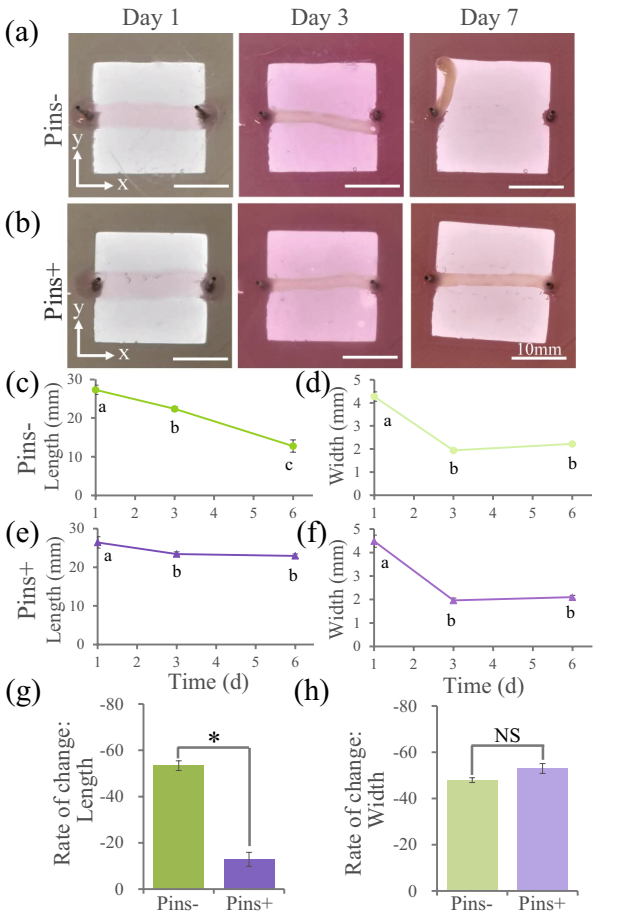

Fig. 6 Dimensional measurement of bio-cultured artificial muscle (BiCAM) on days 1–7. **a**, **b** States of BiCAM on days 1, 3, and 7 without and with pins, respectively. Scale bars, 10 mm. **c**–**h** Mean ± SD values were calculated from four samples. **c**, **e** The BiCAM length with respect to culture days with and without pins, respectively. **d**, **f** The BiCAM width with respect to culture days with and without pins, respectively. **c**–**e** ANOVA test followed by a Scheffe test. $p < 0.05$. Identical letters indicate no significant difference. **f** Tamhane's T2 Test. $p < 0.05$. Identical letters indicate no significant difference. **g** Rate of change in length. **h** Rate of change in width. **g**, **h** Statistical test: *U* test. *NS* not significant, * $p < 0.05$

of BiCAM cultured without and with Pins (Pins− vs. Pins+ (Proposed)) were measured. Figure 6a, b are images of the BiCAM on days 1–7 of incubation. We observed that BiCAM Pins− shrank over time, whereas BiCAM with Pins did not (Fig. 6a, b). The lengths and widths were compared on days 1, 3, and 6 of incubation and statistical analysis examined whether there was a significant difference in the widths and lengths among culture days (Fig. 6c–f). As shown in Fig. 6c, the BiCAM length becomes shorter as the number of culture days increases in Pins− condition. In contrast, BiCAM Pins+ did not have a significant difference in length between days 3 and 6. In addition, the rate of change was calculated to examine the effect of the pins on muscle length (Fig. 6g). The rate of change in length was lower in Pins− condition than in the Pins+ condition (Fig. 6g, *U* test, $p < 0.05$) showing BiCAM spontaneously shrinks in Pins− condition. Furthermore, we investigated the pins effect on the BiCAM width and calculated the rate of change in width because narrower width of the bioactuators has been shown to result in higher maturity [35]. The BiCAM width did not change post day 3 in both conditions.

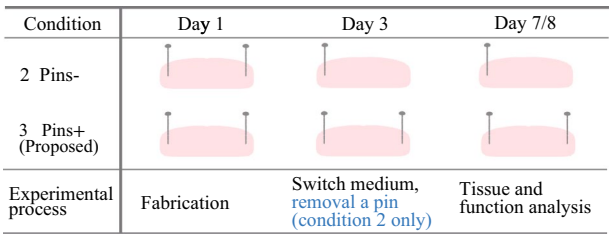

Fig. 5 Schematic representation of the experimental procedure using I-shaped BiCAM. Bioactuators were fabricated on day 1. On the third day, half the samples were removed from one of the pins and subsequently referred to as without pins (Pins−) samples. The remaining samples were kept in the proposed condition (Pins+). On day 7 or 8, cell alignment analysis by immunostaining and functional investigation were performed

Although there was no significant difference (Fig. 6h, U test, $p > 0.05$), the rate of change in width was lower in the Pins+ condition (Ave. 42.04%) than in the Pins− treatment (Ave. 52.07%). These results indicate that the proposed method contributes to the shape maintainable and it also may induce cell maturation.

4.2 BiCAM Shows Cell Alignment in the Long-Axis Direction

To evaluate the alignment of cells in the tissue, antibody staining was performed using MHC for visualization of muscle cells. MHC is a protein expressed in myotubes and muscle fibers [36]. Myoblasts exert contractile force by becoming myotubes and muscle fibers after differentiation and fusion. The BiCAM was stained with anti-MHC antibody and observed using a confocal microscope (Fig. 7a–d). The MHC signal Pins− is darker than that under the Pins+ condition, suggesting more advanced muscle cell development (Fig. 7a–d). We observed that the cell alignment in the Pins− condition was random (Fig. 7a, c) or y-axis (short axis, data not shown) whereas that of the cells in Pins+ condition was along the x-axis (long-axis, Fig. 7b, d). To quantitatively evaluate the cell alignment, we analyzed the confocal images (Fig. 7c, d) and created color maps (Fig. 7e, f). Color maps indicate cell alignment direction. The direction of the cells in the part indicated by the red squares in Fig. 7e and f is shown in the histogram (Fig. 7g, h). The histogram was plotted binning the direction of the cells into 10° bins. Figure 7e, f show that there is more variation in the color map for Pins− condition than in that of the Pins+ condition. Analysis of variance in cell alignment was performed under these two conditions using the Watson–Williams test. We discovered that there was a significant difference in the variability between Pins− and Pins+ ($p < 0.001$). BiCAM Pins+ has less variation in the cell direction. These results indicate that the alignment of cells was induced by our proposed method and that cell alignment is predictable, i.e., controllable.

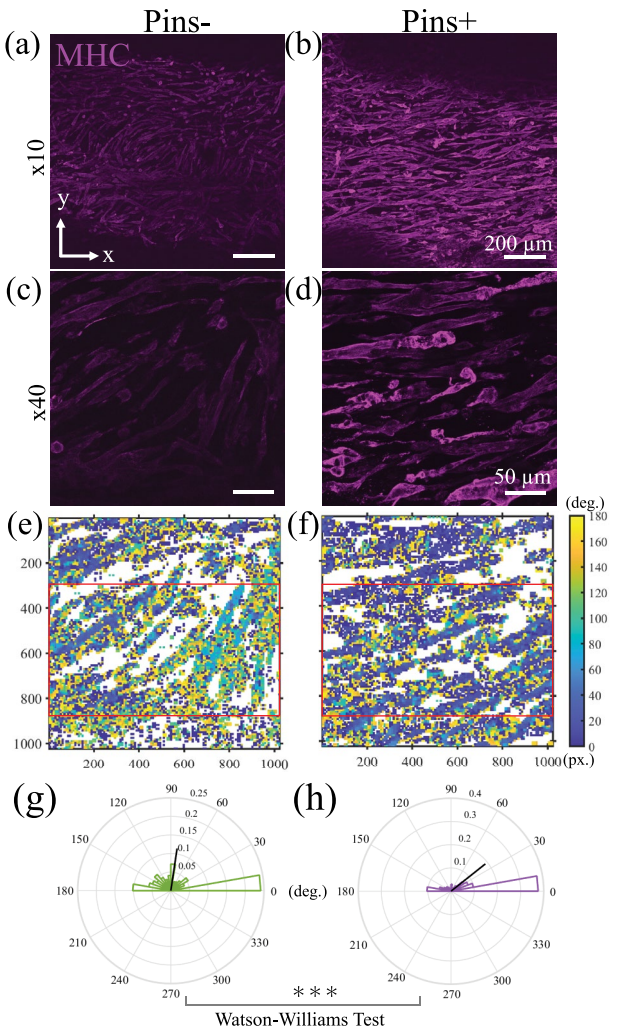

Fig. 7 Evaluation of myotube alignment by immunostaining. **a–d** Myosin heavy chain (MHC) immunostaining with bio-cultured artificial muscle (BiCAM). **a**, **b** Observation with a 10× lens. Scale bars, 200 μm. **c**, **d** Observation with 40× lens. Scale bars, 50 μm. **e**, **f** Color map of cell alignment direction (degree) using Fig. 4c, d. Red square indicates region of interest (ROI) for histogram in Fig. 4g, h. **g**, **h** A histogram of the cell alignment (degree). Watson–Williams test. ***$p < 0.001$. **a**, **c**, **e**, **g** BiCAM without pins (Pins−). **b**, **d**, **f**, **h** BiCAM with pins (Proposed, Pins+)

4.3 BiCAM with Proposed Condition Acts as an Actuator

Bioactuators function by contracting in response to external stimuli [9–14]. We measured BiCAM length as index of muscle contraction to investigate whether BiCAM under the proposed condition shows contraction in response to electrical stimulation. Figure 8a, b show the results of 1 and 50 Hz, respectively. These figures show typical examples. In the case of 1 Hz, BiCAM showed contraction in all five stimulations (Fig. 8a, supplementary video 1). In the case of 50 Hz, BiCAM showed two contractions, one at the beginning and one at the end of stimulation. Greater contraction

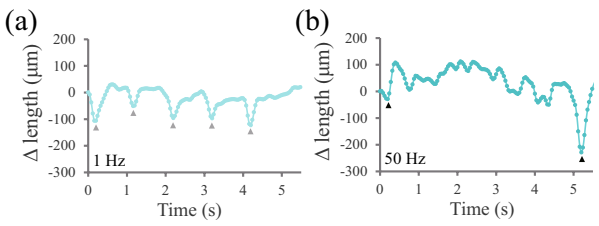

Fig. 8 Analysis of bio-cultured artificial muscle (BiCAM) contraction in response to electrical stimulation. Arrow heads indicate a presence of contraction. Duration time, 10 ms. **a** 1 Hz. **b** 50 Hz

was observed in the latter (Fig. 8b, supplementary video 2). Because BiCAM in the proposed method contracted by external stimulus, it can be used for bioactuator.

4.4 Modeling and Frequency Response Analysis of BiCAM

We quantitatively investigate the characteristics of BiCAM by modeling and frequency response analysis. Considering the future use of BiCAM as a robot actuator, we analyze it from a viewpoint of control theory. We expect to be able to control BiCAM in the same way as an actuator such as a motor.

We model the BiCAM with electric stimulation as input and displacement as output. Considering the behavior of BiCAM (Fig. 8a), there is a damper that suppresses rapid contraction and a spring that tries to undo the contraction for a muscle with a certain mass, it can be replaced as a spring–mass–damper system as shown below;

$$m\ddot{x} + c\dot{x} + kx = f, \tag{1}$$

where let x and f denote BiCAM displacement and input, respectively. Because the relationship between force and voltage is proportional, we use voltage for f. We defined the base parameter $\boldsymbol{a}$ and regressor $\boldsymbol{\xi}$ with Eqs. (2) and (3), respectively, to identify the unknown parameters in equation (1).

$$\boldsymbol{a} = \begin{bmatrix} m & c & k \end{bmatrix}^T \tag{2}$$

$$\boldsymbol{\xi} = \begin{bmatrix} \ddot{x} & \dot{x} & x \end{bmatrix} \tag{3}$$

To estimate the unknown parameters, we used data with periodic stimuli of 1 Hz (duration: 10 ms). As a result, each parameter was estimated to be $m = 0.0$ g, $c = 66$ μN s/m and $k = 1.1$ mN/m. The parameter estimation results show that only the spring and damper terms have values, indicating that BiCAM can also be represented by Hill's muscle model [37], which is known as the most general model of muscle. Comparison of the response of the modeled BiCAM to the impulse input and the experimental data shows a considerable similarity, suggesting that the estimation of the unknown parameters was successful (Fig. 9a).

Investigation of the frequency response characteristics of the modeled BiCAM shows that there is a decay in amplitude at 20 rad/s (about 3.14 Hz, Fig. 9b). The phase diagram shows that there is a significant delay for high-frequency stimuli. This confirms that the periodic stimulation at 1 Hz does not cause a delay in the displacement output, but that the 50 Hz experiment produced the displacement with delay after the last stimulus (Fig. 8). In other words, BiCAM responds to periodic stimuli at about 3 Hz without attenuation or delay, but may not respond correctly to higher frequencies. This indicates that BiCAM should be restricted to stimuli below 3 Hz to control BiCAM.

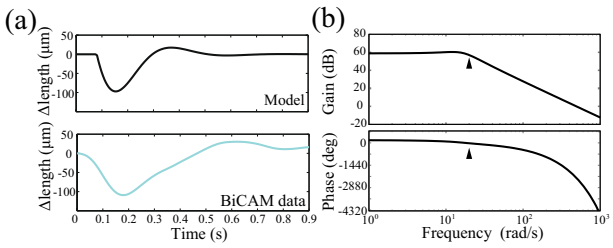

Fig. 9 Behavior and frequency response characteristics of modeled BiCAM. **a** Response of BiCAM when impulse input is applied. The black line shows the modeled BiCAM and the blue line shows the actual BiCAM behavior. **b** Bode diagram of BiCAM

5 Discussion

In this study, we tried to establish an easy fabrication method of bioactuator having high design flexibility without bio3D printer. We proposed the method using dish with a combination of pins and a mold. We called three-dimensional cultured muscle cells in this study BiCAM (bio-cultured artificial muscle). BiCAM using proposed method keep shape, and it showed that cell alignment and contraction in response to electrical stimulus. These results met to our criteria which need our purpose. We also showed that the final shape and the cell orientation when culturing tissue under more needle in Y-shaped BiCAM, suggesting any shape can be fabricated with our purposed method (Figs. 3, 4). We concluded our proposed method is an easy fabrication method of bioactuator having high design flexibility. Moreover, we can control the final shape and the cell orientation and these property are same in each sample, suggesting our method can standardize bioactuators.

Myoblasts are progenitor cell of skeletal muscle. They form 3D tissue after mature and cell fusion induced by differentiation in living animals and *in vitro*. Three-dimensional cultured muscle cells also need two phases—proliferation and differentiation. Shrinkage of Y-shaped BiCAM in without Pins condition was observed during proliferation (Fig. 3). This result is as same as Huang et al. reported. We also performed detailed shape analysis using I-shaped BiCAM (Fig. 6). In the detailed analysis, we removed a pin from BiCAM as Pins− condition during differentiation (Fig. 5). Shrinkage of I-shaped BiCAM in Pins− condition was observed during induction of differentiation (Fig. 3), whereas shrinkage of BiCAMs in the proposed (Pins+) condition was not observed (Figs. 3, 6). These data indicate that the proposed method acts on

both proliferation and differentiation phase and inhibits shrinkage by cell dynamics.

We checked cell alignment by a phase contrast microscope in light field (Y-shaped, Fig. 4) and by confocal microscope with immunostaining (I-shaped, Fig. 7). ECM for Y-shaped BiCAM is collagen, whereas ECMs for I-shaped BiCAM are Matrigel and fibrinogen mainly. Although ECMs for Y-shaped and I-shaped were different, cell alignment of long-axis were induced by the proposed method (Figs. 4, 7). Therefore, our proposed method can induce cell alignment in three-dimensional cultured muscle cells regardless of ECM. Though, contraction force is changed by combination of ECM components [38]. Indeed, contraction of BiCAM composed in response to electrical stimulus by collagen only was not observed (data not shown).

When the muscle contraction to electrical stimulation was examined, it was observed that the muscles responded immediately to each stimulus at 1 Hz and contracted twice at 50 Hz, once at the beginning and once at the end of the stimulus (Fig. 8). The second length at 50 Hz was larger than the length of the first contraction. The modeling and the frequency response analysis based on the experimental results at 1 Hz showed that there was an immediate response and a constant contraction length up to 3.14 Hz input, but there is a delay in the response and the contraction length decrease at higher Hz (Fig. 9). Compared with the experimental results, high frequency cannot be represented by Hill's model (spring–damper system), suggesting that high frequency should be represented by other non-linear mathematical models. Since only length to electrical stimulation (1 and 50 Hz) was measured in this study, we will measure the contraction force of BiCAM and analyze it in detail for model building.

We will do the following for robotic applications in future research. We used C2C12 myoblast cells in this study. Because three-dimensional cultured muscle cells using primary myoblast were much more mature than that of C2C12 [39], we aim to further improve the contractile force of BiCAM using primary myoblast. When three-dimensional cultured muscle cells are used for muscle cell robot, bioactuators are cultured while mounted on the robot components [11–14]. This is because it is difficult to embed mature three-dimensional cultured muscle cells to robot without damage and loss. Thus, we will unitize BiCAM and develop muscle robot.

6 Conclusion

Bionics can create artificial tissue and organs using living cells. These technologies enable to develop biohybrid robots (e.g., muscle cell robot). The accompanying bioprinting technology has also been developed in relation to bionics. However, bioprinting technology requires a lot of experience and skill. Therefore, the aim of this study was to develop a easy method for fabricating bioactuators with high design flexibility. In order to establishment of the method, we have set three criteria in this study: (i) shape maintenance, (ii) cell alignment, and (iii) contraction in response to external stimuli. Results showed that proposed method was able to set and maintain the shape of three-dimensional cultured muscle. We named three-dimensional cultured muscle cells in this study BiCAM (bio-cultured artificial muscle). The BiCAMs incubated in the proposed method show cell alignment and contraction in response to electrical stimulation like biological muscle. These results indicate that our proposed method satisfies all three criteria set. Thus, we concluded that our proposed method is the method for fabricating bioactuators with high design flexibility.

Supplementary Information The online version contains supplementary material available at https://doi.org/10.1007/s42235-023-00355-9.

Acknowledgements This work was partially supported by Japan Society for the Promotion of Science (JSPS) KAKENHI Grant Numbers JP18H05467, JP19K23488. We would like to thank Dr. Y. Morimoto and Dr. K. Furusawa for providing technical advice, and Dr. M. Kojima for technical support.

Data Availability The datasets generated and analyzed during the current study are available from the corresponding author on reasonable request.

Declarations

Conflict of interest The authors have no competing interests to declare that are relevant to the content of this article.

References

1. Wang, J. X., Gao, D., & Lee, P. S. (2021). Recent progress in artificial muscles for interactive soft robotics. *Advanced Materials, 33*(19), e2003088. https://doi.org/10.1002/adma.202003088
2. He, Q. S., Yin, G. X., Vokoun, D., Shen, Q., Lu, J., Liu, X. F., Xu, X. R., Yu, M., & Dai, Z. D. (2022). Review on improvement, modeling, and application of ionic polymer metal

composite artificial muscle. *Journal of Bionic Engineering, 19*, 279–298. https://doi.org/10.1007/s42235-022-00153-9
3. Ricotti, L., Trimmer, B., Feinberg, A. W., Raman, R., Parker, K. K., Bashir, R., Sitti, M., Martel, S., Dario, P., & Menciassi, A. (2017). Biohybrid actuators for robotics: A review of devices actuated by living cells. *Science Robotics, 2*(12), eaaq0495. https://doi.org/10.1126/scirobotics.aaq0495
4. Gao, L., Akhtar, M. U., Yang, F., Ahmad, S., He, J. K., Lian, Q., Cheng, W., Zhang, J. H., & Li, D. C. (2021). Recent progress in engineering functional biohybrid robots actuated by living cells. *Acta Biomaterialia, 121*, 29–40. https://doi.org/10.1016/j.actbio.2020.12.002
5. Lin, Z. N., Jiang, T., & Shang, J. Z. (2021). The emerging technology of biohybrid micro-robots: A review. *Bio-Design and Manufacturing, 5*, 107–132. https://doi.org/10.1007/s42242-021-00135-6
6. Nawroth, J. C., Lee, H., Feinberg, A. W., Ripplinger, C. M., McCain, M. L., Grosberg, A., Dabiri, J. O., & Parker, K. K. (2012). A tissue-engineered jellyfish with biomimetic propulsion. *Nature Biotechnology, 30*(8), 792–797. https://doi.org/10.1038/nbt.2269
7. Chan, V., Park, K., Collens, M. B., Kong, H. J., Saif, T. A., & Bashir, R. (2012). Development of miniaturized walking biological machines. *Scientific Reports, 2*, 857. https://doi.org/10.1038/srep00857
8. Park, S. J., Gazzola, M., Park, K. S., Park, S., Di Santo, V., Blevins, E. L., Lind, J. U., Campbell, P. H., Dauth, S., Capulli, A. K., Pasqualini, F. S., Ahn, S., Cho, A., Yuan, H. Y., Maoz, B. M., Vijaykumar, R., Choi, J. W., Deisseroth, K., Lauder, G. V., … Parker, K. K. (2016). Phototactic guidance of a tissue-engineered soft-robotic ray. *Science, 353*(6295), 158–162. https://doi.org/10.1126/science.aaf4292
9. Kabumoto, K., Hoshino, T., Akiyama, Y., & Morishima, K. (2013). Voluntary movement controlled by the surface EMG signal for tissue-engineered skeletal muscle on a gripping tool. *Tissue Engineering Part A, 19*(15–16), 1695–1703. https://doi.org/10.1089/ten.TEA.2012.0421
10. Akiyama, Y., Sakuma, T., Funakoshi, K., Hoshino, T., Iwabuchi, K., & Morishima, K. (2013). Atmospheric-operable bioactuator powered by insect muscle packaged with medium. *Lab on a Chip, 13*(24), 4870–4880. https://doi.org/10.1039/c3lc50490e
11. Cvetkovic, C., Raman, R., Chan, V., Williams, B. J., Tolish, M., Bajaj, P., Sakar, M. S., Asada, H. H., Saif, M. T., & Bashir, R. (2014). Three-dimensionally printed biological machines powered by skeletal muscle. *Proceedings of the National Academy of Sciences of the United States of America, 111*(28), 10125–10130. https://doi.org/10.1073/pnas.1401577111
12. Raman, R., Cvetkovic, C., Uzel, S. G., Platt, R. J., Sengupta, P., Kamm, R. D., & Bashir, R. (2016). Optogenetic skeletal muscle-powered adaptive biological machines. *Proceedings of the National Academy of Sciences of the United States of America, 113*(13), 3497–3502. https://doi.org/10.1073/pnas.1516139113
13. Morimoto, Y., Onoe, H., & Takeuchi, S. (2018). Biohybrid robot powered by an antagonistic pair of skeletal muscle tissues. *Science Robotics, 3*(18), eaat4440. https://doi.org/10.1126/scirobotics.aat4440
14. Guix, M., Mestre, R., Patiño, T., De Corato, M., Fuentes, J., Zarpellon, G., & Sánchez, S. (2021). Biohybrid soft robots with self-stimulating skeletons. *Science Robotics, 6*(53), eabe7577. https://doi.org/10.1126/scirobotics.abe7577
15. Shima, A., Morimoto, Y., Sweeney, H. L., & Takeuchi, S. (2018). Three-dimensional contractile muscle tissue consisting of human skeletal myocyte cell line. *Experimental Cell Research, 370*(1), 168–173. https://doi.org/10.1016/j.yexcr.2018.06.015
16. Yi, H. G., Kim, H., Kwon, J., Choi, Y. J., Jang, J., & Cho, D. W. (2021). Application of 3D bioprinting in the prevention and the therapy for human diseases. *Signal Transduction and Targeted Therapy, 6*(1), 177. https://doi.org/10.1038/s41392-021-00566-8
17. Jamieson, C., Keenan, P., Kirkwood, D., Oji, S., Webster, C., Russell, K. A., & Koch, T. G. (2021). A review of recent advances in 3D bioprinting With an eye on future regenerative therapies in veterinary medicine. *Frontiers in Veterinary Science, 7*, 584193. https://doi.org/10.3389/fvets.2020.584193
18. Ostrovidov, S., Salehi, S., Costantini, M., Suthiwanich, K., Ebrahimi, M., Sadeghian, R. B., Fujie, T., Shi, X., Cannata, S., Gargioli, C., Tamayol, A., Dokmeci, M. R., Orive, G., Swieszkowski, W., & Khademhosseini, A. (2019). 3D bioprinting in skeletal muscle tissue engineering. *Small, 15*(24), e1805530. https://doi.org/10.1002/smll.201805530
19. Kang, D. H., Louis, F., Liu, H., Shimoda, H., Nishiyama, Y., Nozawa, H., Kakitani, M., Takagi, D., Kasa, D., Nagamori, E., Irie, S., Kitano, S., & Matsusaki, M. (2021). Engineered whole cut meat-like tissue by the assembly of cell fibers using tendon-gel integrated bioprinting. *Nature Communications, 12*(1), 5059. https://doi.org/10.1038/s41467-021-25236-9
20. Shimizu, K., Fujita, H., & Nagamori, E. (2009). Alignment of skeletal muscle myoblasts and myotubes using linear micropatterned surfaces ground with abrasives. *Biotechnology and Bioengineering, 103*(3), 631–638. https://doi.org/10.1002/bit.22268
21. Heher, P., Maleiner, B., Prüller, J., Teuschl, A. H., Kollmitzer, J., Monforte, X., Wolbank, S., Redl, H., Rünzler, D., & Fuchs, C. (2015). A novel bioreactor for the generation of highly aligned 3D skeletal muscle-like constructs through orientation of fibrin via application of static strain. *Acta Biomaterialia, 24*, 251–265. https://doi.org/10.1016/j.actbio.2015.06.033
22. Huang, Y. C., Dennis, R. G., Larkin, L., & Baar, K. (2005). Rapid formation of functional muscle in vitro using fibrin gels. *Journal of Applied Physiology, 98*(2), 706–713. https://doi.org/10.1152/japplphysiol.00273.2004
23. Vandenburgh, H. H., Hatfaludy, S., Karlisch, P., & Shansky, J. (1989). Skeletal muscle growth is stimulated by intermittent stretch-relaxation in tissue culture. *The American Journal of Physiology, 256*(3 Pt 1), C674–C682. https://doi.org/10.1152/ajpcell.1989.256.3.C674
24. Fujita, H., Nedachi, T., & Kanzaki, M. (2007). Accelerated de novo sarcomere assembly by electric pulse stimulation in C2C12 myotubes. *Experimental Cell Research, 313*(9), 1853–1865. https://doi.org/10.1016/j.yexcr.2007.03.002
25. Ito, A., Yamamoto, Y., Sato, M., Ikeda, K., Yamamoto, M., Fujita, H., Nagamori, E., Kawabe, Y., & Kamihira, M. (2014). Induction of functional tissue-engineered skeletal muscle constructs by defined electrical stimulation. *Scientific Reports, 4*, 4781. https://doi.org/10.1038/srep04781
26. Kim, H., Kim, M. C., & Asada, H. H. (2019). Extracellular matrix remodelling induced by alternating electrical and mechanical stimulations increases the contraction of engineered skeletal muscle tissues. *Scientific Reports, 9*(1), 2732. https://doi.org/10.1038/s41598-019-39522-6
27. Madden, L., Juhas, M., Kraus, W. E., Truskey, G. A., & Bursac, N. (2015). Bioengineered human myobundles mimic clinical responses of skeletal muscle to drugs. *eLife, 4*, e04885. https://doi.org/10.7554/eLife.04885
28. Schneider, C. A., Rasband, W. S., & Eliceiri, K. W. (2012). NIH Image to ImageJ: 25 years of image analysis. *Nature Methods, 9*(7), 671–675. https://doi.org/10.1038/nmeth.2089
29. Faustino Martins, J. M., Fischer, C., Urzi, A., Vidal, R., Kunz, S., Ruffault, P. L., Kabuss, L., Hube, I., Gazzerro, E., Birchmeier, C., Spuler, S., Sauer, S., & Gouti, M. (2020). Self-organizing 3D human trunk neuromuscular organoids. *Cell Stem Cell, 26*(2), 172-186.e6. https://doi.org/10.1016/j.stem.2019.12.007

30. Kaehler, A., & Bradski, G. (2016). *Learning OpenCV 3: Computer vision in C++ with the OpenCV library* (p. 992). O'Reilly Media Inc.
31. Sherman, M. T., Wang, H. T., Garfinkel, S. N., & Critchley, H. D. (2022). The cardiac timing toolbox (CaTT): Testing for physiologically plausible effects of cardiac timing on behaviour. *Biological Psychology, 170*, 108291. https://doi.org/10.1016/j.biopsycho.2022.108291
32. Yamasaki, K., Hayashi, H., Nishiyama, K., Kobayashi, H., Uto, S., Kondo, H., Hashimoto, S., & Fujisato, T. (2009). Control of myotube contraction using electrical pulse stimulation for bio-actuator. *Journal of Artificial Organs, 12*(2), 131–137. https://doi.org/10.1007/s10047-009-0457-4
33. Ikeda, K., Ito, A., Sato, M., Kawabe, Y., & Kamihira, M. (2016). Improved contractile force generation of tissue-engineered skeletal muscle constructs by IGF-I and Bcl-2 gene transfer with electrical pulse stimulation. *Regenerative Therapy, 3*, 38–44. https://doi.org/10.1016/j.reth.2015.12.004
34. Kane, G. A., Lopes, G., Saunders, J. L., Mathis, A., & Mathis, M. W. (2020). Real-time, low-latency closed-loop feedback using markerless posture tracking. *eLife, 9*, e61909. https://doi.org/10.7554/eLife.61909
35. Morimoto, Y., Kato-Negishi, M., Onoe, H., & Takeuchi, S. (2013). Three-dimensional neuron-muscle constructs with neuromuscular junctions. *Biomaterials, 34*(37), 9413–9419. https://doi.org/10.1016/j.biomaterials.2013.08.062
36. Schmidt, M., Schüler, S. C., Hüttner, S. S., von Eyss, B., & von Maltzahn, J. (2019). Adult stem cells at work: Regenerating skeletal muscle. *Cellular and Molecular Life Sciences CMLS, 76*(13), 2559–2570. https://doi.org/10.1007/s00018-019-03093-6
37. Winters, J. M. (1990). Hill-based muscle models: A systems engineering perspective. *Multiple muscle systems* (pp. 69–93). Springer.
38. Hinds, S., Bian, W., Dennis, R. G., & Bursac, N. (2011). The role of extracellular matrix composition in structure and function of bioengineered skeletal muscle. *Biomaterials, 32*(14), 3575–3583. https://doi.org/10.1016/j.biomaterials.2011.01.062
39. Langelaan, M. L., Boonen, K. J., Rosaria-Chak, K. Y., van der Schaft, D. W., Post, M. J., & Baaijens, F. P. (2011). Advanced maturation by electrical stimulation: Differences in response between C2C12 and primary muscle progenitor cells. *Journal of Tissue Engineering and Regenerative Medicine, 5*(7), 529–539. https://doi.org/10.1002/term.345